European Journal of Control 58 (2021) 357–372

Contents lists available at ScienceDirect

European Journal of Control

journal homepage: www.elsevier.com/locate/ejcon

*L*1 adaptive backstepping control for path-following of underactuated marine surface ships

Haitong Xu[a], P. Oliveira[b], C. Guedes Soares[a,*]

[a] *Centre of Marine Technology and Ocean Engineering (CENTEC), Instituto Superior Técnico, Universidade de Lisboa, Av. Rovisco Pais, 1049-001 Lisboa, Portugal*

[b] *Associated Laboratory for Energy, Transports and Aeronautics, Instituto Superior Técnico, Universidade de Lisboa, Av. Rovisco Pais, 1049-001 Lisboa, Portugal*

ARTICLE INFO

Article history:
Received 16 January 2020
Revised 13 July 2020
Accepted 8 August 2020
Available online 14 August 2020

Recommended by Prof. T. Parisini

Keywords:
L1 adaptive control
Vector field
Underactuated ship
Path-following
Stability analysis

ABSTRACT

A *L1* adaptive backstepping controller is proposed for path-following control of an underactuated ship based on a nonlinear steering model, and the control law is derived using Lypunov control function. *L1* adaptive controller is a novel technology considering both the robustness and fast adaptation. The closed-loop control system is proved to be uniformly global asymptotically stable. A novel guidance law, time-varying vector field, is proposed for the guidance system. The kinematic analysis of path-following shows that the guidance and control systems are coupled, and the guidance system is affected by the performance of the controller. The Lyapunov method is employed to show that the equilibrium point of the whole system is uniformly global asymptotically stable. Path-following simulations are carried out to validate the performance of the proposed control law and vector field guidance law using a fully nonlinear manoeuvring mode of an underactuated tanker in the presence of stochastic ocean current.

1. Introduction

Marine autonomous surface ships (MASS) have been drawing much attention in the maritime industry, and this is reflected in the recent guidelines for the conduct of autonomous ship trials approved by the Maritime Safety Committee (MSC) of the International Maritime Organisation (IMO) in 2019. The main reasons for the rapid development of autonomous ships are safety and economic benefit. The direct causes of ship losses are of different nature [17], but different studies have concluded that about 75% to 96% of marine accidents can be traced back to human errors [1,18]. Autonomous shipping can significantly improve safety by reducing human errors. Another driving force for the development of autonomous or unmanned ships is an economic benefit. Autonomous ships can significantly reduce the cost of onboard personnel and fuel consumption, although initial investment in equipment and shore based support maybe higher [46]. Meanwhile, without the Life support system, the ship can carry more cargos.

These important benefits have motivated recent research on autonomous ships. For example, Rolls-Royce [45] led a project that addressed the various factors related to the development of autonomous ships, such as economic, social, regulatory and technology. In the following year, Norway opens an official test bed for autonomous shipping [35]. In 2018, IMO defined degrees of autonomy for autonomous surface ships, and the preliminary research on the regulation of autonomous ships was carried out. For an autonomous ship, the most important and fundamental system is the guidance and control system as it directly affects the whole performance of autonomous ships.

A robust and reliable guidance and control system are closely related to the safety of autonomous ships. The research on the guidance and control system of autonomous ships is becoming important and urgent, especially with the fast development of autonomous ships.

A review in the area of nonlinear controllers for ships can be found in [11], which briefly introduced the application of the nonlinear controllers, such as linear quadratic regulator (LQR), state feedback linearization, backstepping, sliding mode control, etc. In recent years, model predictive control was used for surface ships by Oh and Sun [39], where the rudder dynamic model was considered. A sliding mode controller was used for trajectory tracking of an ROV by Guerrero et al. [20]. Liu et al. [33] used the model predictive control for the path following control of a marine surface ship considering the roll motion effect. Meanwhile, experiments were carried to validate the proposed control law. Fuzzy logic control was widely used in autonomous systems due to the simple control structure. Li et al. [31] used an adaptive neural network

* Corresponding author.
E-mail address: c.guedes.soares@centec.tecnico.ulisboa.pt (C. Guedes Soares).

https://doi.org/10.1016/j.ejcon.2020.08.003
0947-3580/

fast power reaching for the path following control of underactuated marine surface vessels. A review on the fuzzy logic control for marine underwater vehicles can be found in Xiang et al. [51]. Wang et al. [50] proposed a fuzzy observer-based controller for surface ships, and globally asymptotically stable was proved.

The adaptive control method is one promising technology for a dynamic system, especially for autonomous ships because the marine surface ships usually travel in a complex environmental with waves, wind, and currents. The classical control system is designed using a static steering model, for example, the Nomoto model, which is the most widely used. The static steering model does not consider the time-varying environmental disturbance and thus it usually will fail to describe the ship's dynamic response when the environment changes [42]. For example, when ships access a harbour from the ocean, the pilots can feel that the ship is becoming hard to manoeuvre. In fact, research shows that the shallow water has a significant effect on the manoeuvrability of ships [26,48]. Unfortunately, the classical controller based on static steering models does not consider the effect of shallow water, which changes the manoeuvring model (Xu and Guedes Soares, 2019).

Recently, a novel adaptive control architecture, denoted as *L1* adaptive control, was proposed. It can guarantee both fast adaptation and transient performance, as described in [21]. Guerreiro, Silvestre, Cunha, Cao, and Hovakimyan [19] used *L1* adaptive controller for an inner loop controller for autonomous rotorcraft. Kaminer et al. [23] employed the *L1* adaptive controller for the path-following of unmanned aerial vehicles. Lee et al. [28] proposed an *L1* adaptive backstepping controller for autopilot of an agile missile. Sørensen and Breivik [47] compared the performance of *L1* adaptive backstepping controller with the classical adaptive control. The results show that the *L1* adaptive control has a better performance. Some published papers demonstrate that the *L1* adaptive control greatly improved the performance of unmanned aerial vehicles, such as, [16,19,24,28]. In this paper, *L1* adaptive backstepping controller is employed for the path-following control problem of an underactuated ship.

Guidance and control system are the basic component for an autonomous ship. The guidance portion of the system is used to develop the variable input signal, which represents the desired course to the target. There are many guidance laws for an autonomous system, such as pure pursuit (PP), vector field (VF) [57], constant bearing (CB) and line of sight (LOS). LOS is one popular method, and widely used for autonomous ships [3,14,15,30,36,49]. Lekkas and Fossen [30], proposed a revised version of LOS, look-ahead LOS, for the autonomous ships, where the look-ahead distance is a time-varying function of the cross-track error. Follow-up work can be found in [37]. An integral LOS (ILOS) was proposed to compensate the drift forces due to environmental disturbance [3,12,29]. LOS guidance law is a geometry method, because the desired heading angle is determined with a triangle, which consists of the location of the ship, path, and look-ahead distance.

Vector field guidance law is a mathematical method that was proposed by borrowing the concept of potential flow. Vector field generates the vectors near the path, and the vectors indicate the desired course angle. When the ship follows the vectors, she will converge to the desired path. The core part of the vector field guidance law is the mathematical function that defines the vectors. It was used for autonomous air vehicles [27,38]. Recently, the vector field method has been used for path-following control of autonomous ships [52,53], and shows a good performance. One advantage of the vector field is its flexible structure. It calculates the desired heading angle using a vector generation function, which can be defined with the requirement of the tasks, for example, arrival angle [32], trajectory-tracking [27], obstacles avoidance.

The guidance and control system are a typical coupled nonlinear system, and the stability properties need to be analysed. The most desired stability for a closed-loop nonlinear system is global exponential stable (GES) [2,25,34], because the convergence of the error dynamic equations is bounded by an exponential decay. However, unfortunately, it cannot be achieved for path-following control of autonomous ships. The kinematics of the path-following introduces saturation through trigonometric functions [13].

Global κ-exponential stability of LOS guidance law was firstly proved by Fredriksen and Pettersen [15]. Fossen and Pettersen [13] gave the proof of uniform semiglobal exponential stability (USGES) for LOS guidance law. Do et al. [7] used a robust adaptive controller for path-following control of underactuated ships. The following works can found in [5,8,9],

In this paper, *L1* adaptive backstepping controller is proposed for path-following control, and the performance is evaluated with a fully nonlinear manoeuvring model of an underactuated autonomous ship. The key feature of *L1* adaptive-control architectures is the decoupling of estimation and control, which enables the use of arbitrarily fast estimation rates without sacrificing robustness. A nonlinear steering model considering the environmental disturbance is employed for the control system design. The Lyapunov control function is used to derive the control law, where the parameter update law is also given. The stability proof shows that the L1 adaptive backstepping controller is a uniform global asymptotic stable (UGAS). The guidance system is designed based on the vector field method, and a time-varying vector field guidance law is proposed. The coupled guidance and control system are proved to be uniform global asymptotic stable (UGAS) using a cascaded system theory. The proposed control law and guidance law are validated with a fully nonlinear manoeuvring mode in the presence of stochastic ocean current.

This paper is organized as follows. Sections 2 describes the kinematic of path-following control for an underactuated marine surface ship. Section 3 proposed the *L1* adaptive backstepping controller and stability proof is also outlined. The parameters update law is also given in this section. In Section 4, the error dynamic equations of the guidance and control system are summarised, and the theorem and proof for UGAS are given using cascaded system theory. Section 5 presented the path-following simulations. The performance of the proposed guidance and control system is discussed. Conclusions are given in Section 6.

2. Problem formulation

Path-following control of marine surface ships is briefly introduced in this section. As presented in Fig. 1, a typical path-following control system consists of path generation (waypoints), guidance law, controller and the marine craft. Here, several assumptions are given. First, the drift angle β can be directly measured. As discussed in [29], the drift angle can be measured using a global navigation satellite system an inertial navigation system and inertial measurement unit. Second, the velocities of the ship can be measured correctly.

This paper considers the straight path, where the path tangential angle is constant. Fig. 2 shows the geometric information of two-dimensional path-following control for a marine craft. The red line is the predefined path. Two coordinate frames are defined in this figure. The straight path, which connects the predefined way points (x_j, y_j), $j = 1 \cdots N$, is defined in the North-East-Down (NED) coordinate frame. The body-fixed frame is a moving coordinate frame that is fixed to the craft. The ship motions, such as surge and sway speed (u,v), are measured in the body-fixed frame. The path-tangential frame is a moving coordinate frame, whose origin is the projection of the ship's centre of gravity (x_p, y_p). γ_p is the path tangential angle. The yaw angle and position are measured relative to the NED frame.

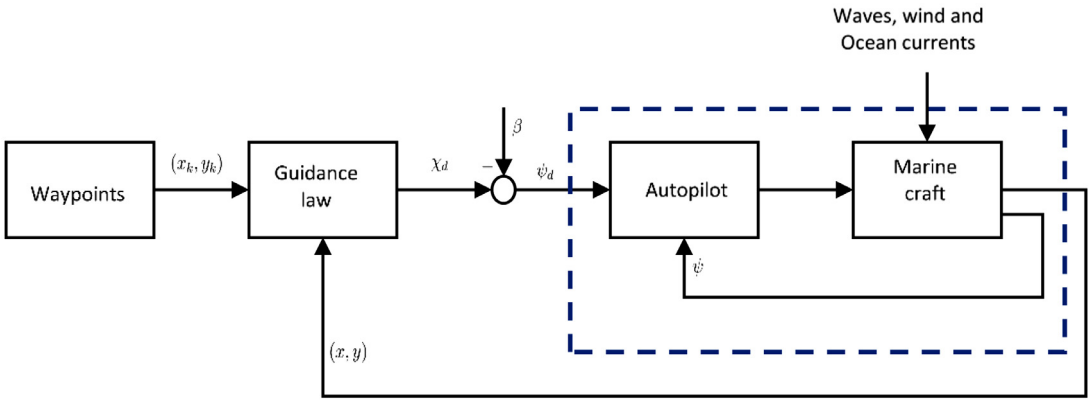

Fig. 1. Marine control system for path following, where the path is defined by waypoints; β is the drift angle.

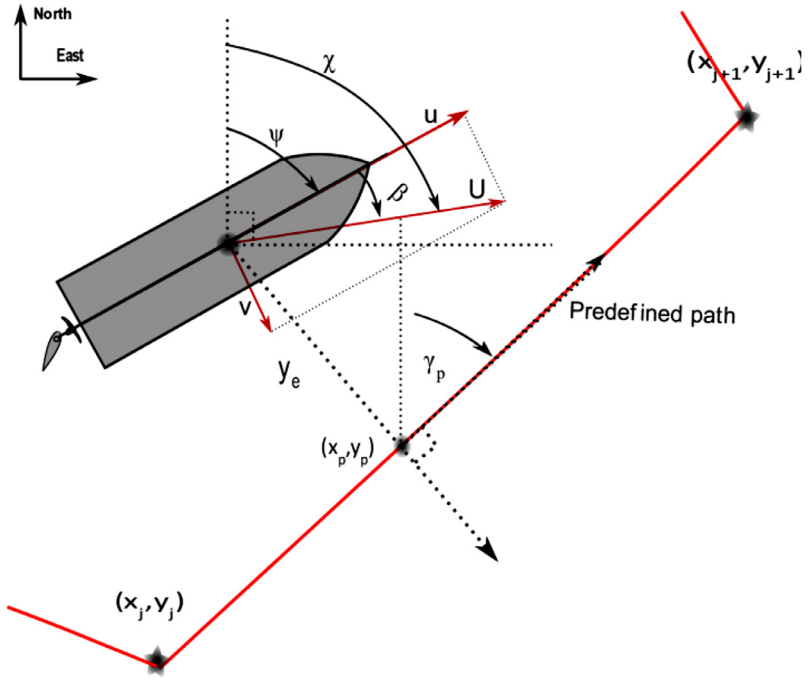

Fig. 2. Geometry description of two-dimensional path-following.

2.1. Path-following control objective

As presented in Fig. 2, the path connects the N waypoints (x_j, y_j) for $j = 1, \cdots, N$. The cross-track error y_e is the distance between the ship and the predefined path. From Fig. 2, the equations of cross-track error is given:

$$\begin{bmatrix} 0 \\ y_e \end{bmatrix} = \mathbf{R}(\gamma_p) \begin{bmatrix} x(t) - x_p(t) \\ y(t) - y_p(t) \end{bmatrix} \tag{1}$$

where, $(x(t), y(t))$ is the ship's location in real-time, $(x_p(t), y_p(t))$ is the projection of the centre of the ship. γ_p is the path tangential angle. $\mathbf{R}(\gamma_p)$ is the rotation matrix, and given as:

$$\mathbf{R}(\gamma_p) = \begin{bmatrix} \cos(\gamma_p) & -\sin(\gamma_p) \\ \sin(\gamma_p) & \cos(\gamma_p) \end{bmatrix} \in SO(2) \tag{2}$$

Expanding (1), leads to the cross-track error y_e:

$$y_e(t) = -(x(t) - x_p(t)) \sin(\gamma_p) + (y(t) - y_p(t)) \cos(\gamma_p) \tag{3}$$

Obviously, the control object of the path-following is to make cross-track error converge to zero. It is given as:

$$\lim_{t \to +\infty} y_e(t) = 0 \tag{4}$$

2.2. Kinematic-error equations of path-following

Considering a ship moving in a horizontal plane, the kinematic equations of a marine surface vessel moving in 3DOF (surge, sway, and yaw) can be described:

$$\begin{aligned} \dot{x} &= u \cos(\psi) - v \sin(\psi) \\ \dot{y} &= u \sin(\psi) + v \cos(\psi) \\ \dot{\psi} &= r \end{aligned} \tag{5}$$

Differentiation of the Eq. (3), gives:

$$\begin{aligned} \dot{y}_e &= -\dot{x} \sin(\gamma_p(\theta)) + \dot{y} \cos(\gamma_p(\theta)) \\ &= U \sin(\psi - \gamma_p(\theta) + \beta) \end{aligned} \tag{6}$$

It can be further simplified by substituting Eq. (5) into Eq. (6), resulting:

$$\dot{y}_e = U \sin(\psi - \gamma_p + \beta) \tag{7}$$

where, U is the ground speed of a ship, $(U = \sqrt{u^2 + v^2})$. The β is the drift angle $\beta = \text{atan2}(v, u)$. Finally, the time differential, y_e, becomes:

$$\dot{y}_e = U \sin(\chi - \gamma_p) \tag{8}$$

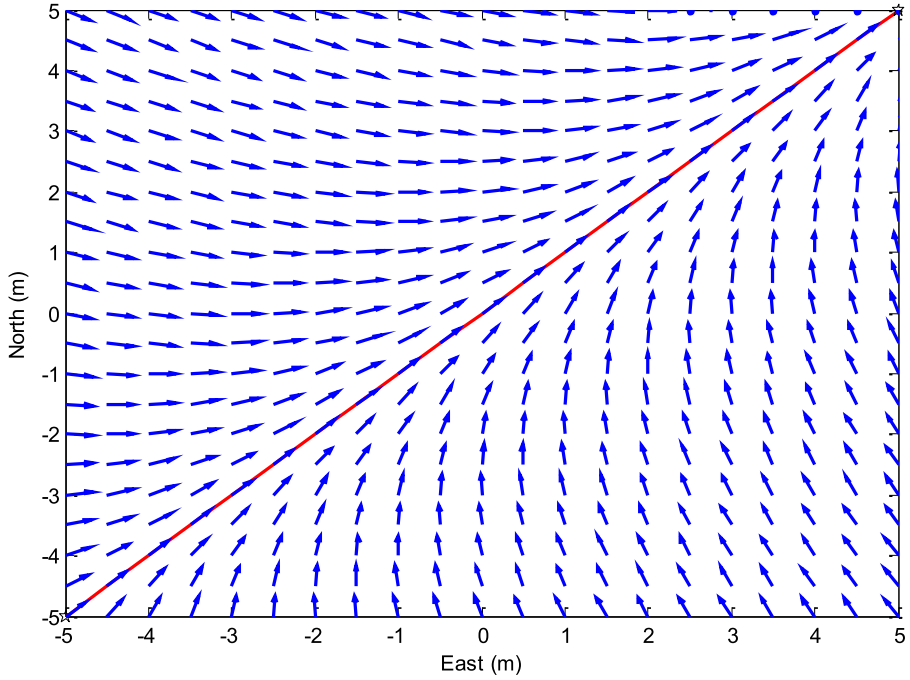

Fig. 3. Vectors around the straight path.

where the $\chi = \psi + \beta$ is the course angle of the ship.

The principle of vector field method is to generate vectors towards the predefined path. The vectors denote the desired travelling direction for the autonomous vessels, as presented in Fig. 3. A guidance law is used to generate the vector around the desired path (red line). The vectors indicate the reference heading (course) angle for the control system. Obviously, if the ship tracks the vectors successfully, it will converge to the path finally. In this paper, vector field method is chosen as the guidance law. Here, a time-varying vector field guidance law is proposed:

$$\begin{aligned}\chi_d &= \gamma_p - \tan^{-1}\left(\mathrm{sgn}(y_e)\frac{|y_e|^{\theta(t,y_e)}}{\Delta}\right)\\ &= \gamma_p - \mathrm{sgn}(y_e)\tan^{-1}\left(\frac{|y_e|^{\theta(t,y_e)}}{\Delta}\right)\end{aligned} \tag{9}$$

where $\theta(t, y_e)$ is a time-varying function and $\Delta > 0$ is a predefined constant and $0 < \Delta_{\min} < \Delta < \Delta_{\max}$. The function, $\theta(t, y_e)$, is defined as:

Definition 1. The function $\theta(t, y_e)$ is a non-decreasing positive semi-definite function and $\theta(t, y_e = 0) \geq 1$. Furthermore, $\theta'(t, y_e) \geq 0$.

Remark. . The function, $\theta(t, y_e)$ plays an important role in the proposed guidance law. It controls the convergence rate. In order to make sure the errors converge fast, the function $\theta(t, y_e)$ should increase with the variable, y_e. It means that the system has a higher convergence rate when y_e is large. It can also be chosen as a constant value. For example, if $\theta(t, y_e) = 1$, then the vector field guidance law degenerate to the classical LOS guidance law.

The heading tracking error satisfies:

$$\tilde{\psi} = \psi - \psi_d = \chi - \chi_d == \tilde{\chi} \tag{10}$$

With the Eqs. (9) - (10), the Eq. (7) can be simplified:

$$\dot{y}_e = U\sin\left(\tilde{\psi} - \mathrm{sgn}(y_e)\tan^{-1}\left(\frac{|y_e|^{\theta(t,y_e)}}{\Delta}\right)\right) \tag{11}$$

Expanding the formula gives:

$$\begin{aligned}\dot{y}_e = {} & U\sin\left(\tilde{\psi}\right)\cos\left(\tan^{-1}\left(\frac{|y_e|^{\theta(t,y_e)}}{\Delta}\right)\right)\\ & - \mathrm{sgn}(y_e)U\cos\left(\tilde{\psi}\right)\sin\left(\tan^{-1}\left(\frac{|y_e|^{\theta(t,y_e)}}{\Delta}\right)\right)\end{aligned} \tag{12}$$

It can be further simplified as:

$$\dot{y}_e = \underbrace{-\mathrm{sgn}(y_e)\frac{U|y_e|^{\theta(t,y_e)}}{\sqrt{\Delta^2 + |y_e|^{2\theta(t,y_e)}}}}_{f_1(t,y_e)} + \underbrace{U\phi\left(t, y_e, \tilde{\psi}\right)\tilde{\psi}}_{g(t,y_e,\tilde{\psi})} \tag{13}$$

where $\phi(t, y_e, \tilde{\psi})$ is defined as:

$$\begin{aligned}\phi\left(t, y_e, \tilde{\psi}\right) = {} & \frac{\sin\left(\tilde{\psi}\right)}{\tilde{\chi}}\frac{\Delta}{\sqrt{\Delta^2 + |y_e|^{2\theta(t,y_e)}}}\\ & - \mathrm{sgn}(y_e)\frac{\cos\left(\tilde{\psi}\right) - 1}{\tilde{\chi}}\frac{|y_e|^{\theta(t,y_e)}}{\sqrt{\Delta^2 + |y_e|^{2\theta(t,y_e)}}}\end{aligned} \tag{14}$$

3. *L1* adaptive controller for heading

In this section, the *L1* adaptive controller is proposed for the heading control of autonomous ships. The classical autopilot for ships is usually designed based on Nomoto model. It is a linearized manoeuvring model, and describes the yaw dynamic response to the rudder steering. The oversimplified structure decreases the accuracy of the yaw motion's prediction. So, in this paper, a nonlinear Nomoto model with bounded environmental disturbance is chosen:

$$\begin{aligned}\dot{\psi} &= r\\ T^*\dot{r} + H^*(r)r &= K^*\delta + b^*\end{aligned} \tag{15}$$

where, T^* and K^* are the Nomoto constants. They can be estimated using a system identification method resorting for instance to zigzag manoeuvring test [43,44,56]. $H^*(r) = 1 + a_2 r^2$, is the positive nonlinear damping term. δ is the rudder angle. $b^* \leq b_{max}$

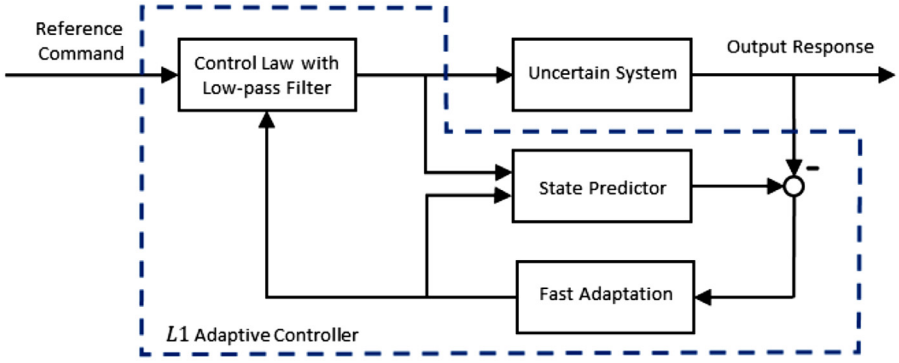

Fig. 4. Block diagram of the *L1* adaptive controller.

represent the environmental disturbance. Assume there are uncertainties associated with the parameters. The relationship between the real and estimated parameter is assumed as:

$$\begin{aligned} T^* &= \eta T \\ H^*(r) &= \sigma H(r) \\ K^* &= \rho K \end{aligned} \tag{16}$$

where, $\eta \in \mathbb{R}^+, \sigma \in \mathbb{R}^+, \rho \in \mathbb{R}^+$ are the uncertainties associated with the T, H(r) and K, respectively. Additionally, it is assumed that the uncertainty and environmental disturbance, b^*, is slowly varying relative to the ship dynamics, the derivative of the uncertainty is negligible, (i.e. $\dot{\eta} = 0, \dot{\sigma} = 0, \dot{\rho} = 0$, and, $\dot{b}^* = 0$). Substituting (16) into (15) gives:

$$\begin{aligned} \dot{\psi} &= r \\ \eta T \dot{r} + \sigma H(r) r &= \rho K \delta + b^* \end{aligned} \tag{17}$$

3.1. State predictor with adaptation laws

Fig. 4 shows the block diagram of *L1* adaptive controller. It consists mainly of a state predictor, parameters adaptation, and control law with low-pass filter. In the following part, a *L1* adaptive backstepping controller is proposed, and the control law is given. The parameter adaption laws are derived first. The stability proof for the closed-loop control system is also presented and UGAS is proved. The control law is derived using the backstepping method [10,28].

Given a state predictor, the prediction errors are:

$$\tilde{\psi} = \hat{\psi} - \psi; \tilde{r} = \hat{r} - r \tag{18}$$

where, $\hat{\psi}$ and $\hat{r}$ are the estimated value, respectively. The ideal prediction errors are defined as:

$$\dot{\tilde{\psi}}_{ideal} = -\Gamma_1 \tilde{\psi}; \dot{\tilde{r}}_{ideal} = -\Gamma_2 \tilde{r} \tag{19}$$

where, Γ_1 and Γ_2 are positive constants, which render their equilibrium point exponentially stable. Then the state prediction is defined as:

$$\begin{aligned} \dot{\hat{\psi}} &= -\Gamma_1 \tilde{\psi} + r \\ \dot{\hat{r}} &= -\Gamma_2 \tilde{r} + T^{-1}\left(\hat{\rho}_\eta K \delta + \hat{b}^*_\eta - \hat{\sigma}_\eta H(r) r\right) \end{aligned} \tag{20}$$

where, $\hat{\rho}_\eta = \hat{\rho}/\hat{\eta}$, $\hat{\sigma}_\eta = \hat{\sigma}/\hat{\eta}$, $\hat{b}^*_\eta = \hat{b}^*/\hat{\eta}$, and the superscript represents the estimated value, and $\hat{\eta}$ is assumed positive, i.e. $\hat{\eta} \in \mathbb{R}^+$. A candidate Lyapunov function is used to design the adaption laws for the uncertainties. The prediction errors are defined as:

$$\begin{aligned} \dot{\tilde{\psi}} &= -\Gamma_1 \tilde{\psi} \\ \dot{\tilde{r}} &= -\Gamma_2 \tilde{r} + T^{-1}(\tilde{\rho}_\eta K \delta + \tilde{b}^*_\eta - \tilde{\sigma}_\eta H(r) r) \end{aligned} \tag{21}$$

where, $\tilde{\rho}_\eta = \hat{\rho}_\eta - \rho_\eta$ is the error of the parameter ρ_η. $\tilde{b}^*_\eta = \hat{b}^*_\eta - {b_\eta}^*$ is the error of the parameter, ${b_\eta}^*$. $\tilde{\sigma}_\eta = \hat{\sigma}_\eta - \sigma_\eta$ is the error of the parameter σ_η. Then, consider the positive defined Control Lyapunov Function (CLF),

$$V_{pred} = \frac{1}{2}\left(\frac{1}{\gamma_{\rho_\eta}}\tilde{\rho}^2_\eta + \frac{1}{\gamma_{\sigma_\eta}}\tilde{\sigma}^2_\eta + \frac{1}{\gamma_{b_\eta}}\tilde{b^*}_\eta{}^T \tilde{b}^*_\eta\right) + \frac{1}{2}T\tilde{r}^2 + \frac{1}{2}\tilde{\psi}^2 \tag{22}$$

where, γ_{ρ_η},γ_{σ_η} and γ_{b_η} are the adaptation gains. Differentiation of (22) yields:

$$\begin{aligned} \dot{V}_{pred} &= \frac{1}{\gamma_{\rho_\eta}}\tilde{\rho}_\eta \dot{\hat{\rho}}_\eta + \frac{1}{\gamma_{\sigma_\eta}}\tilde{\sigma}_\eta \dot{\hat{\sigma}}_\eta + \frac{1}{\gamma_{b_\eta}}\tilde{b}^*_\eta \dot{\hat{b}}^*_\eta + \tilde{\psi}\dot{\tilde{\psi}} + \tilde{r}T\dot{\tilde{r}} \\ &= \frac{1}{\gamma_{\rho_\eta}}\tilde{\rho}_\eta \dot{\hat{\rho}}_\eta + \frac{1}{\gamma_{\sigma_\eta}}\tilde{\sigma}_\eta \dot{\hat{\sigma}}_\eta + \frac{1}{\gamma_{b_\eta}}\tilde{b}^*_\eta \dot{\hat{b}}^*_\eta - \Gamma_1\tilde{\psi}^2 - T\Gamma_2\tilde{r}^2 \\ &\quad + \tilde{r}\left(\tilde{\rho}_\eta K\delta + \tilde{b}^*_\eta - \tilde{\sigma}_\eta H(r) r\right) \\ &= \tilde{\rho}_\eta\left(\frac{1}{\gamma_{\rho_\eta}}\dot{\hat{\rho}}_\eta + \tilde{r}K\delta\right) + \tilde{\sigma}_\eta\left(\frac{1}{\gamma_{\sigma_\eta}}\dot{\hat{\sigma}}_\eta - \tilde{r}H(r)r\right) \\ &\quad + \tilde{b}^*\left(\frac{1}{\gamma_{b_\eta}}\dot{\hat{b}}^*_\eta + \tilde{r}\right) - \Gamma_1\tilde{\psi}^2 - T\Gamma_2\tilde{r}^2 \end{aligned} \tag{23}$$

From the Eq. (28), the following adaption laws are given:

$$\begin{aligned} \dot{\hat{\rho}}_\eta &= -\gamma_{\rho_\eta}\tilde{r}K\delta \\ \dot{\hat{\sigma}}_\eta &= \gamma_{\sigma_\eta}\tilde{r}H(r)r \\ \dot{\hat{b}}^*_\eta &= -\gamma_{b_\eta}\tilde{r} \end{aligned} \tag{24}$$

In order to prevent parameter drift in adaptation schemes, the projection-based adaptation laws are given:

$$\begin{aligned} \dot{\hat{\rho}}_\eta &= \gamma_{\rho_\eta}\mathrm{Proj}(\rho_\eta, -\tilde{r}K\delta) \\ \dot{\hat{\sigma}}_\eta &= \gamma_{\sigma_\eta}\mathrm{Proj}(\sigma_\eta, \tilde{r}H(r)r) \\ \dot{\hat{b}}^*_\eta &= \gamma_{b_\eta}\mathrm{Proj}(b^*_\eta, -\tilde{r}) \end{aligned} \tag{25}$$

Since the structure of the control law and the definition of the reference model do not change, the tracking error dynamics will be same. The advantage of using projection-type adaptation is that one ensures boundedness of the adaptive parameters [21].

Substituting (24) into (23) gives:

$$\dot{V}_{pred} = -\Gamma_1\tilde{\psi}^2 - T\Gamma_2\tilde{r}^2 \le 0 \tag{26}$$

3.2. Adaptive backstepping control law

In this part, the control law of the adaptive backstepping controller is derived using Lyapunov control function (CLF). For the heading control of autonomous ships, the object is to make $|\psi - \psi_d| \to 0$, where ψ_d is specified by the vector field guidance law. Defining the error variables, z_1 and z_2 as:

$$\begin{aligned} z_1 &= \psi - \psi_d \\ z_2 &= r - \alpha \end{aligned} \tag{27}$$

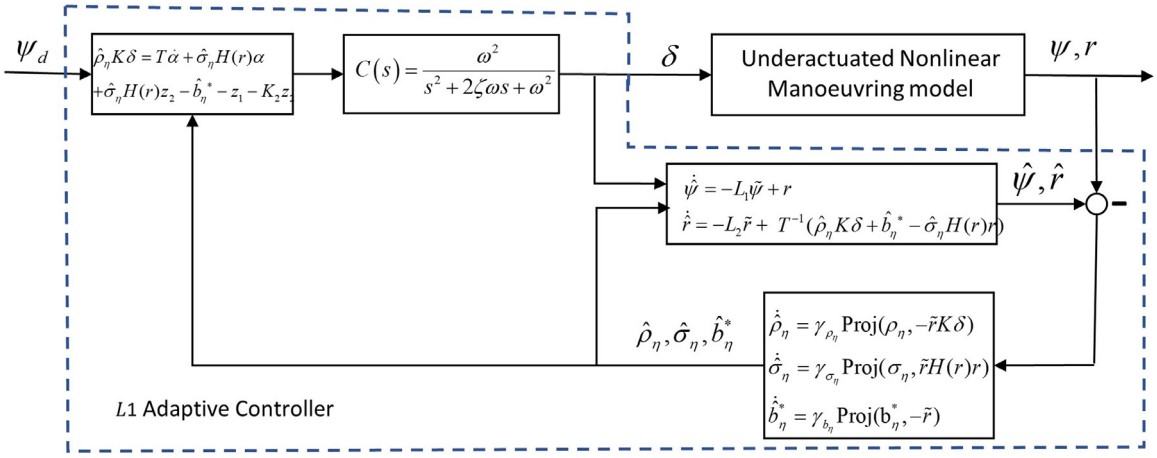

Fig. 5. Closed-loop system of the *L1* adaptive backstepping controller for an underactuated marine surface ship.

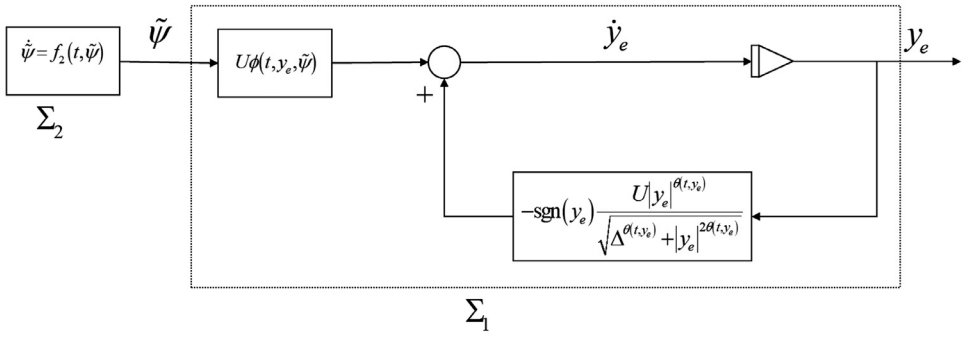

Fig. 6. Error dynamics equations of the guidance and control system.

where, α is a stabilising function. A positive defined CLF is defined as:

$$V_1 = \frac{1}{2}z_1{}^2 \tag{28}$$

The time differential of V_1 is given:

$$\dot{V}_1 = z_1\dot{z}_1 = z_1\left(r - \dot{\psi}_d\right) = z_1 z_2 + z_1\left(\alpha - \dot{\psi}_d\right) \tag{29}$$

Choose the stabilising function, $\alpha = \dot{\psi}_d - K_1 z_1$, and submit intro (29), gives:

$$\dot{V}_1 = -K_1 z^2{}_1 + z_1 z_2 \tag{30}$$

The time differential z_2 is given:

$$T\dot{z}_2 = T\dot{r} - T\dot{\alpha} = \hat{\rho}_\eta K\delta + \hat{b}_\eta^* - \hat{\sigma}_\eta H(r)r - T\dot{\alpha} \tag{31}$$

where, $\dot{\alpha} = \ddot{\psi}_d - K_1\dot{z}_1$. Considering the new variables, z_1 and z_2, the CLF is modified to

$$V_2 = \frac{1}{2}z_2 T^{-1} z_2 + V_1 \tag{32}$$

The derivative of V_{ctrl} is given:

$$\begin{aligned}\dot{V}_2 &= z_2 T^{-1}\dot{z}_2 + \dot{V}_1 = z_2\left(\hat{\rho}_\eta K\delta + \hat{b}_\eta^* - \hat{\sigma}_\eta H(r)r - T\dot{\alpha}\right) \\ &\quad - z_1 K_1 z_1 + z_1 z_2 \\ &= z_2\left(\hat{\rho}_\eta K\delta + \hat{b}_\eta^* - \hat{\sigma}_\eta H(r)r - T\dot{\alpha} + z_1\right) - z_1 K_1 z_1\end{aligned} \tag{33}$$

Submitting, $r = z_2 + \alpha$, into the Eq. (33), resulting,

$$\dot{V}_2 = z_2\left(\hat{\rho}_\eta K\delta + \hat{b}_\eta^* - \hat{\sigma}_\eta H(r)\alpha - T\dot{\alpha} + z_1 - \hat{\sigma}_\eta H(r)\right)z_2 - K_1 z^2{}_1 \tag{34}$$

The control law is given:

$$\hat{\rho}_\eta K\delta = T\dot{\alpha} + \hat{\sigma}_\eta H(r)\alpha - \hat{b}_\eta^* - z_1 + \hat{\sigma}_\eta H(r)z_2 - K_2 z_2 \tag{35}$$

where, $K_2 > 0$. Submitting Eq. (35) into Eq. (34), resulting:

$$\dot{V}_2 = -K_2 z^2{}_2 - K_1 z^2{}_1 \le 0 \tag{36}$$

As discussed above, the parameters $\hat{\rho}_\eta$, $\hat{\sigma}_\eta$ and $\hat{b}_\eta^*$ are adaptive updating using Eq. (24). The CLF considering the parameter uncertainty can be expanded to:

$$\begin{aligned}V_{ctrl} = V_{pred} + V_2 &= \frac{1}{2}\left(\frac{1}{\gamma_{\rho_\eta}}\tilde{\rho}_\eta^2 + \frac{1}{\gamma_{\sigma_\eta}}\tilde{\sigma}_\eta^2 + \frac{1}{\gamma_{b_\eta}}\tilde{b}^*{}_\eta{}^T\tilde{b}_\eta^*\right) \\ &\quad + \frac{1}{2}T\tilde{r}^2 + \frac{1}{2}\tilde{\psi}^2 + \frac{1}{2}z_1{}^2 + \frac{1}{2}z_2 T^{-1} z_2\end{aligned} \tag{37}$$

The derivative of V_{ctrl} becomes:

$$\dot{V}_{ctrl} = \dot{V}_{pred} + \dot{V}_2 = -L_1\tilde{\psi}^2 - TL_2\tilde{r}^2 - \left(K_2 + \hat{\sigma}_\eta H(r)\right)z^2{}_2 - K_1 z^2{}_1 \le 0 \tag{38}$$

From the above discussion, the origin of the error system, $(\tilde{\psi}, \tilde{r}, z_1, z_2, \tilde{\rho}_\eta, \tilde{\sigma}_\eta, \tilde{b}_\eta^*)$, is uniformly globally asymptotically stable (UGAS), [10]. The adaption of uncertainties of parameters may contain high-frequency signals. A low pass filer is applied to control signals [21,47]. It is given as:

$$\delta_{ctrl} = C(s)\delta = \frac{\omega^2}{s^2 + 2\zeta\omega s + \omega^2}\delta \tag{39}$$

where, $C(s)$ is a second-order low-pass filter, $\zeta > 0$ is the damping ratio. $\omega > 0$ is the natural frequency. Fig. 5 shows the closed-loop system of the $C(s)$ is a second-order low-pass filter, $\zeta > 0$ is the damping ratio. $\omega > 0$ is the natural frequency. Fig. 5 shows

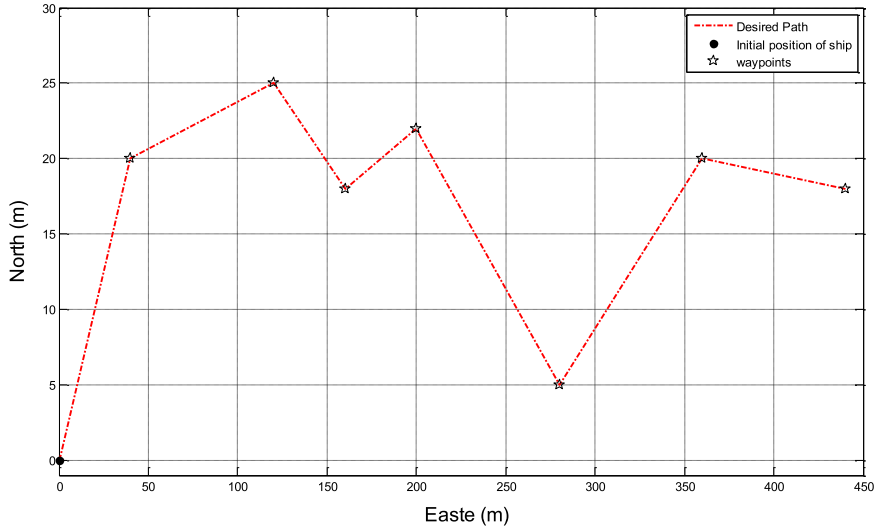

Fig. 7. The geometrical information of a straight path in the NED frame.

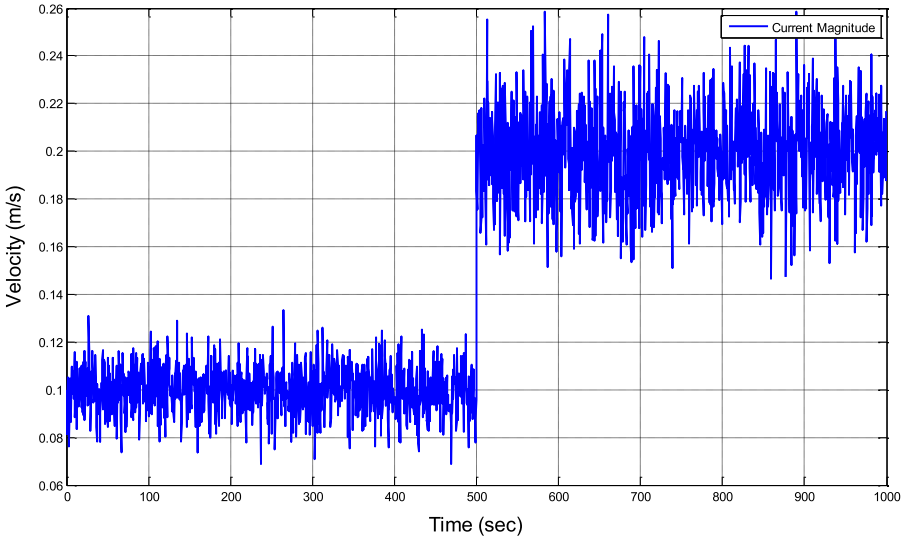

Fig. 8. The magnitude of 2D irrotational stochastic ocean current.

the closed-loop system of the $\mathcal{L}_1$ adaptive backstepping controller. the control law, parameter adaption laws and state estimator are presented in this figure. The underactuated nonlinear manoeuvring model is given the following part.

4. Stability analysis of guidance and control system

The *L1* adaptive backstepping heading controller proposed in the above can be used in cascade with the vector field for path-following control of underactuated ships. If the guidance law in Eq. (9) is chosen, the cross-track error in Eq (13) forms a cascade system, as described in Eqs. (40) and (41). Fig. 6 shows the error dynamics of the cascaded system [4,40,41]. As can be observed, the errors of the heading control system are fed into the error dynamic of the guidance system. It means that the two sub-systems are coupled together. The performance of the controller will directly affect the guidance system.

The error dynamics of the coupled guidance and control system is given:

$$\Sigma_1 : \dot{y}_e = \underbrace{-\mathrm{sgn}(y_e)\frac{U|y_e|^{\theta(t,y_e)}}{\sqrt{\Delta^2+|y_e|^{2\theta(t,y_e)}}}}_{f_1(t,y_e)} + \underbrace{U\phi\left(t,y_e,\tilde{\psi}\right)}_{g(t,y_e,\tilde{\psi})}\tilde{\psi} \tag{40}$$

$$\Sigma_2 : \dot{\tilde{\psi}} = f_2\left(t,\tilde{\psi}\right) \tag{41}$$

where $f_2(t,\tilde{\psi})$ is the heading tracking error dynamics discussed in Section 3, corresponding to Eqs. (20)–(24), (35). From the above discussion, the error dynamic equation of the heading controller, Σ_2, is the driving system. The driving system output the heading errors, which is feed-forward to the driven system, $\Sigma 1$. The driven system is described by Eq. (40), and its performance is affected by the input, $\tilde{\psi}$. In the following phase, the stability property of the proposed guidance and control system is proved by using the cascade system theory.

Property 1. *For a typical marine surface ship, the ground speed is positive and up bounded,*

$$0 < U_{\min} < U < U_{\max}. \tag{43}$$

Based on the above discussion, a theorem is presented and it guarantees that the cascade system Eqs. (40) and (41) of the vector field guidance law and *L1* adaptive backstepping controller is uniformly global asymptotically stable (UGAS).

Theorem 1. *Assume the system Σ_2 are stabilized using the adaptive control law in Eq. (35), where the parameters are dynamically up-*

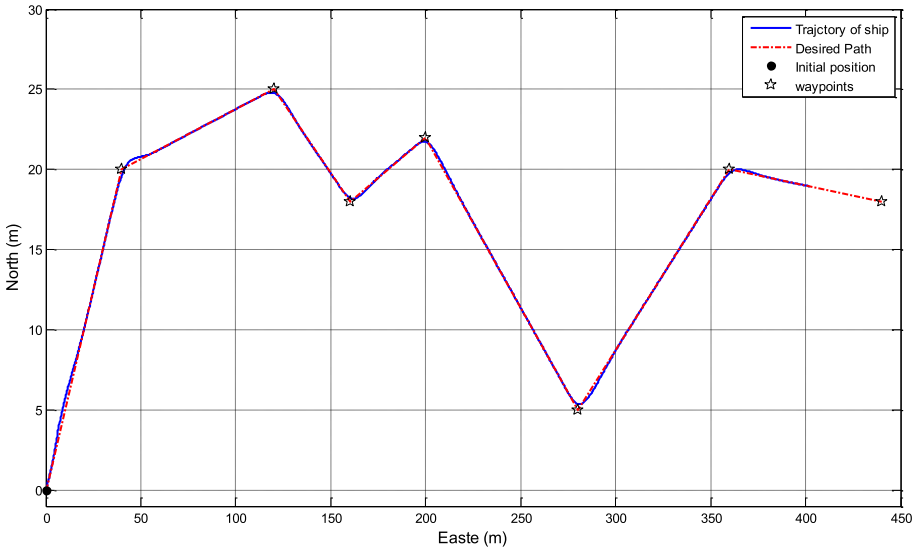

(a) *L1* OFF

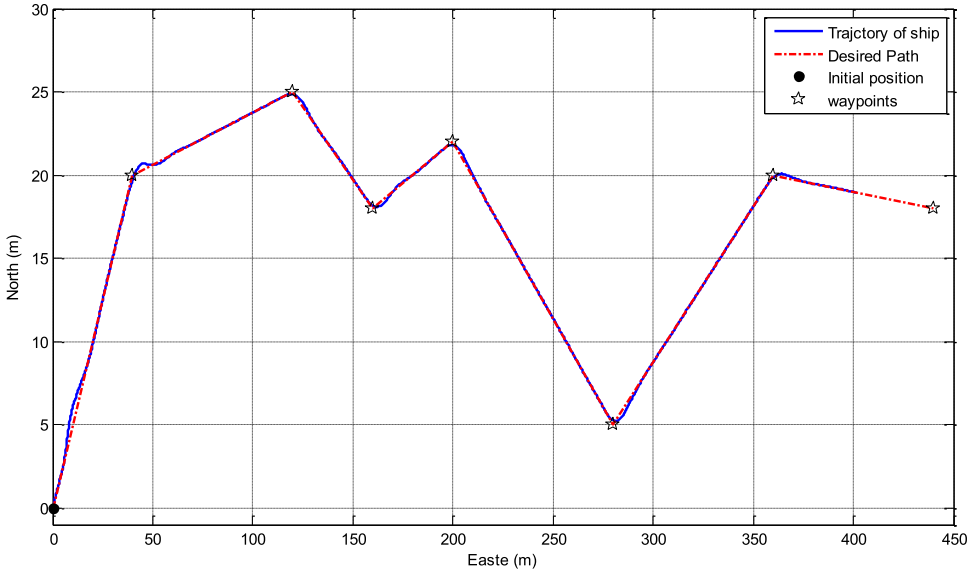

(b) *L1* ON

Fig. 9. The trajectory of the ship model in the simulations.

dated using Eq. (25), the guidance law given by Eq. (9) defines the reference heading angle, ψ_d. Then the equilibrium point $(y_e, \tilde{\psi}) = (0, 0)$ of the coupled guidance and control system (40) - (41) is UGAS, if the function, $\theta(t, y_e)$ satisfies the Definition 1.

Proof. See Appendix A.

5. Simulation

Path-following simulations for an underactuated marine surface ship model will be carried out to evaluate the performance of the proposed guidance and control system. The robustness of the *L1* adaptive backstepping controller with environmental disturbance is emphatically discussed. A 3-DOF (surge, sway and yaw) nonlinear mathematical model of the "Esso Osaka" is chosen to describe the motion of the marine surface ship. This model was validated with sea-trials of full-scale ship test, is quite comprehensive, and it gives highly realistic results [22,37,53,55].

5.1. Nonlinear manoeuvring model

During the simulations, the current force will be considered as the main environmental disturbance for manoeuvring modelling. The effect of the current can be directly included in the mathematical model. The relative forward velocity u_r and transverse velocity v_r are given by:

$$\begin{aligned} u_r &= u - u_c \cos(\psi - \alpha) \\ v_r &= v + u_c \sin(\psi - \alpha) \end{aligned} \tag{44}$$

where, u_c is the magnitude of the current, α is the direction of the

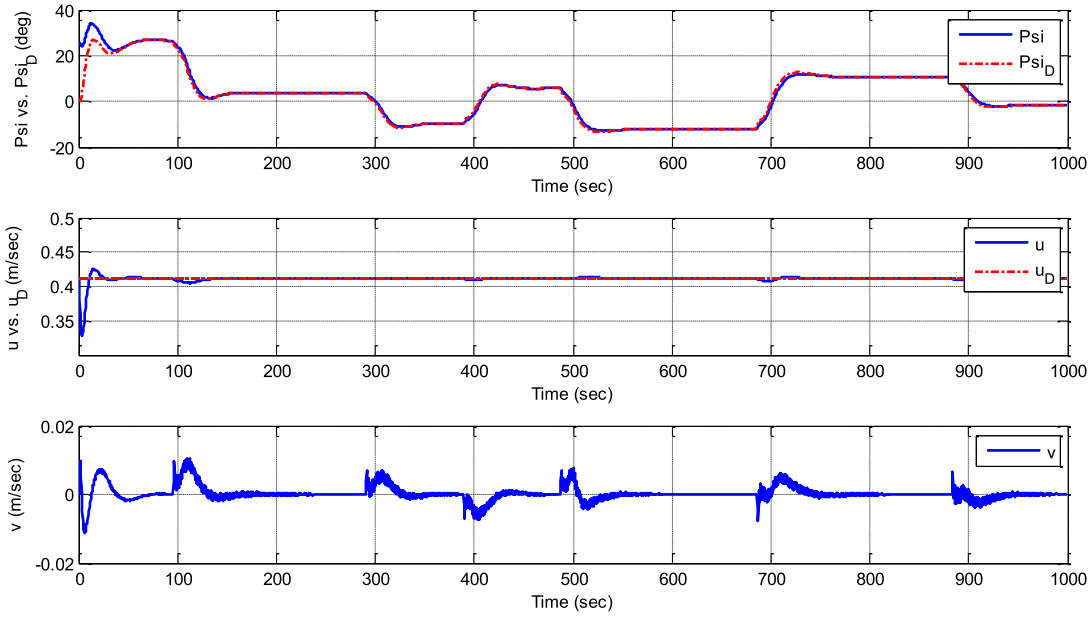

(a) *L1* OFF

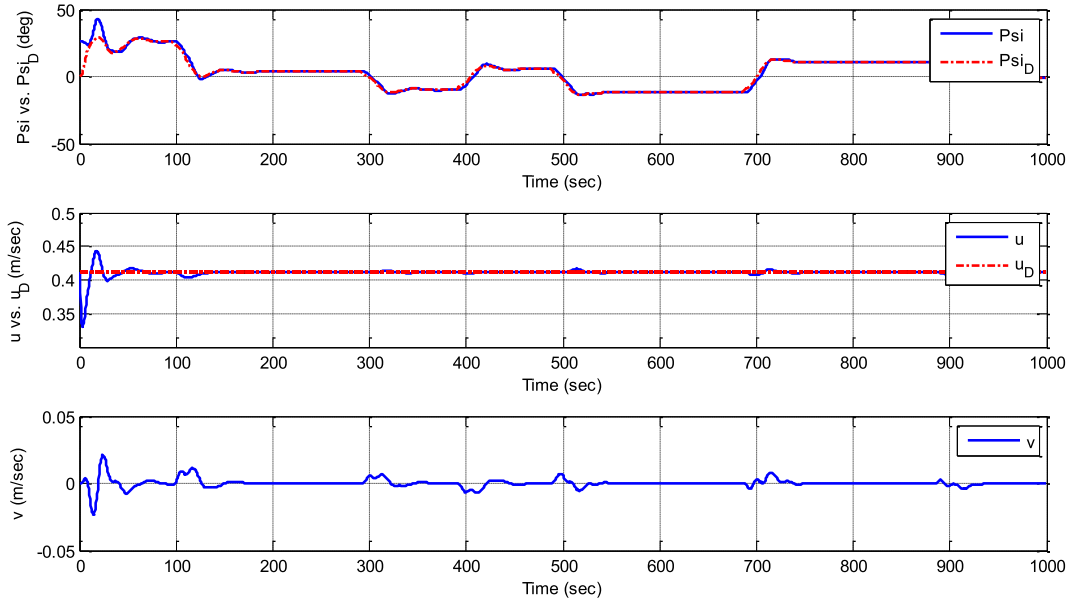

(b) *L1* ON

Fig. 10. The motions (yaw angle, surge speed, sway speed) measured in the simulations.

current. The time derivatives of u and v are given:

$$\begin{cases} \dot{u} = \dot{u}_r - u_c r \sin(\psi - \alpha) \\ \dot{v} = \dot{v}_r - u_c r \cos(\psi - \alpha) \end{cases} \tag{45}$$

where $\dot{u}_r$ and $\dot{v}_r$ are defined by:

$$\begin{cases} \dot{u}'_r = \frac{f'_1}{m' - X'_{\dot{u}_r}} \\ \dot{v}'_r = \frac{1}{f'_4}\left[(I'_z - N'_{\dot{r}})f'_2 - (m'x_G - Y_{\dot{r}}{}')f'_3\right] \\ \dot{r}' = \frac{1}{f'_4}\left[(m' - Y_{\dot{v}_r}{}')f'_3 - (m'x_G - N'_{\dot{v}_r})f'_2\right] \end{cases} \tag{46}$$

where, f'_1, f'_2 and f'_3 are the nondimensionalized hydrodynamic forces and moment. They are defined as:

$$\begin{cases} f'_1 = \eta'_1 u'^2_r + \eta'_2 n' u'_r + \eta'_3 n'^2 - C'_R + X'^2_{v_r} v'^2_r + X'_{e^2} e^2 \\ \quad + \left(X'_{r^2} + m'x'_G\right) r'^2 + \left(X'_{v_r r} + m'\right) v'_r r' + X'_{v_r^2 r^2} v'^2_r r'^2 \\ f'_2 = Y'_0 + \left\{Y'_{v_r} v'_r + Y'_\delta (c - c_0) v'_r\right\} + \left\{\left(Y'_r - m'u'_r\right) r - \frac{Y'_\delta}{2}(c - c_0) r'\right\} \\ \quad + Y'_\delta \delta + Y'_{r^2 v_r} r'^2 v'_r + Y'_{e^3} e^3 \\ f'_3 = N'_0 + \left\{N'_{v_r} v'_r - N'_\delta (c - c_0) v'_r\right\} + \left\{\left(N'_r - m'x'_G u'_r\right) r + \frac{1}{2} N'_\delta (c - c_0) r'\right\} \\ \quad + N'_\delta \delta + N'_{r^2 v_r} r'^2 v'_r + N'_{e^3} e^3 \\ f'_4 = \left(m' - Y'_{\dot{v}_r}\right)\left(I'_z - N'_{\dot{r}}\right) - \left(m'x'_G - N'_{\dot{v}_r}\right)\left(m'x'_G - Y'_{\dot{r}}\right) \end{cases} \tag{47}$$

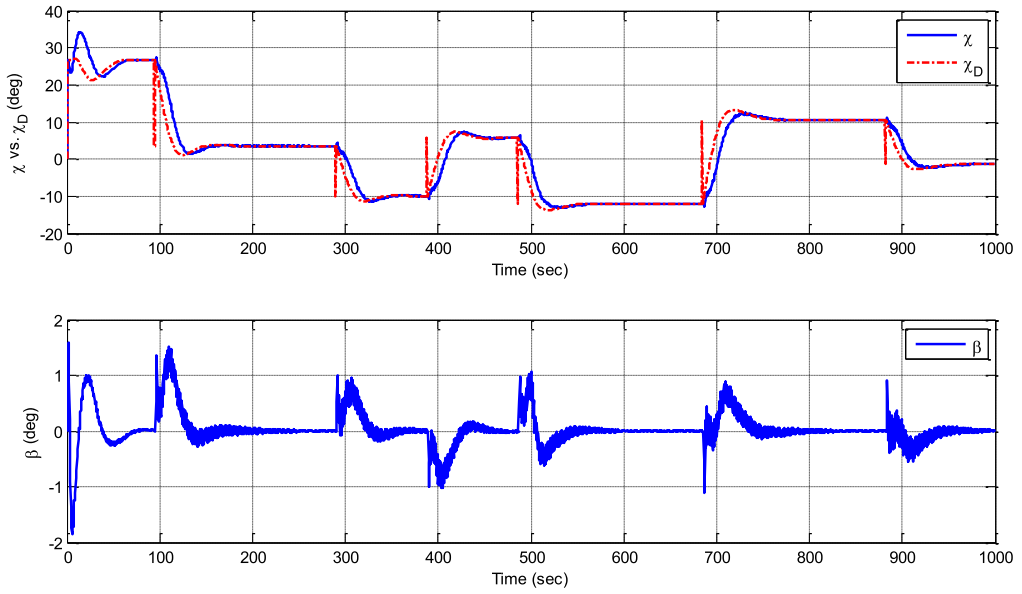

(a) *L1* OFF

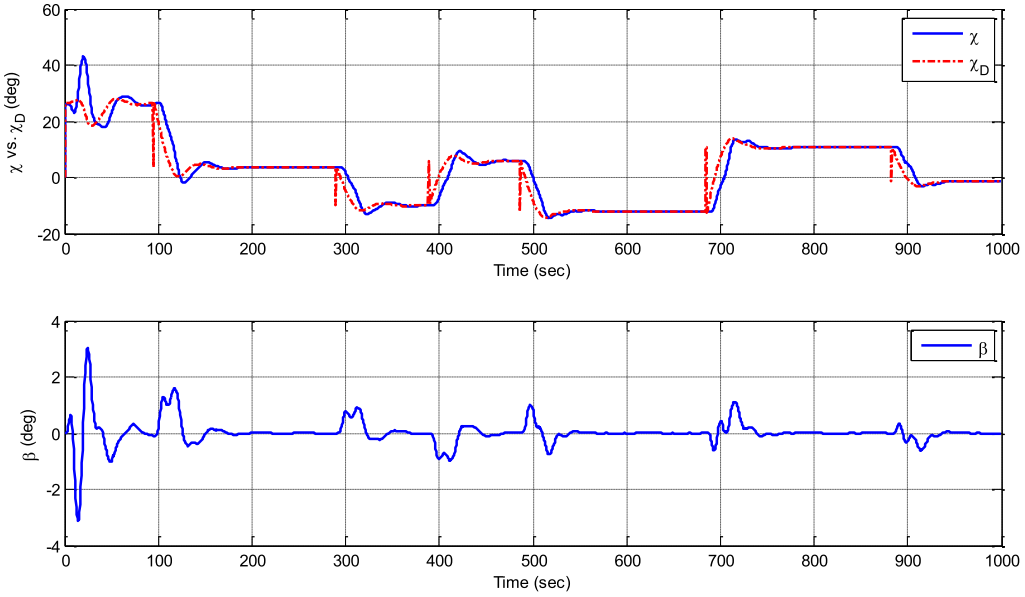

(b) *L1* ON

Fig. 11. The measured course angle and drift angle.

The detailed description of this mathematical model can be found in the [53,54]. The hydrodynamic coefficients in Eq. (47) are presented in Table 1.

5.2. Path-following study

As discussed above, the control objective for path following is to follow a predefined path. In this paper, straight-line is used to connect the waypoints. The waypoints are given: wpt1 = (40, 20), wpt2 = (120, 25), wpt3 = (160, 18), wpt4 = (200, 22), wpt5 = (280, 5), wpt6 = (360, 20), and wpt7 = (440, 18), where the units are meters. The geometrical information of the predefined paths is presented in Fig. 7. There are 8 waypoints. Without loss of generality, they are chosen randomly in a Cartesian coordinate frame.

Table 1
Nondimensional hydrodynamic coefficients of "Esso Osaka" ship model (scale factor = 100).

Coefficient	Value	Coefficient	Value
$(m - Y_{\dot{v}})'$	0.0352	Y'_0	1.90*e-6
$(I_z - N_{\dot{r}})'$	0.00222	Y'_{v_r}	−0.0261
$(m - X_{\dot{u}_r})'$	0.0116	Y'_δ	0.00508
η'_1	−0.962*e-5	Y'_r	0.00365
η'_2	−0.446*e-5	Y'_{rrv_r}	−0.0450
η'_3	0.0309*e-5	Y'_{eee}	−0.00185
C'_R	0.00226	N'_0	−0.00028
$X'_{v_r^2}$	−0.006	N'_{v_r}	−0.0105
X'_{ee}	−0.00224	N'_δ	−0.00283
X'_{rr}	0.00515	N'_r	−0.00480
$(X_{v_r r} + m)'$	0.0266	N'_{rrv_r}	0.00611
X'_{rrw}	−0.00715	N'_{eee}	0.00116

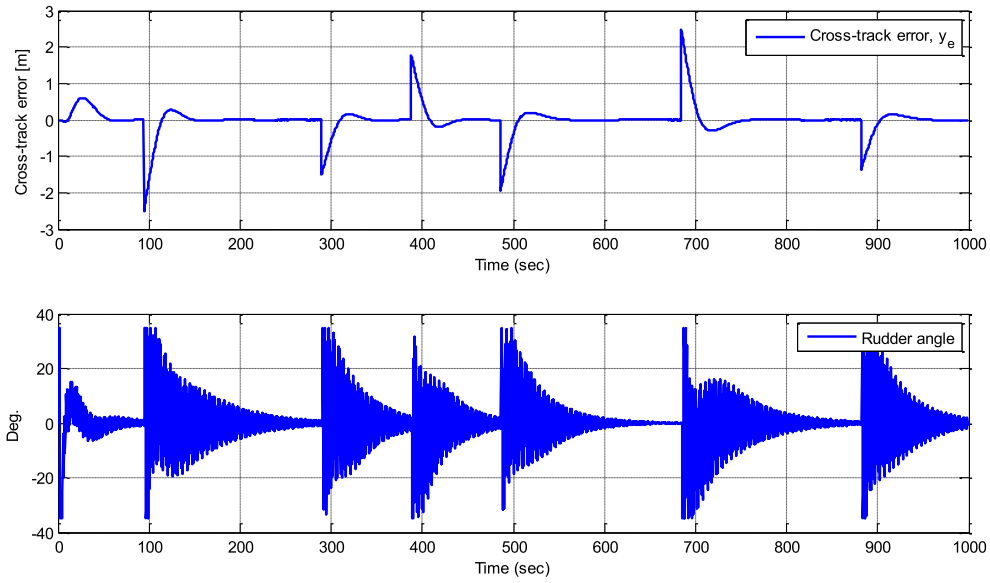

(a) *L1* OFF

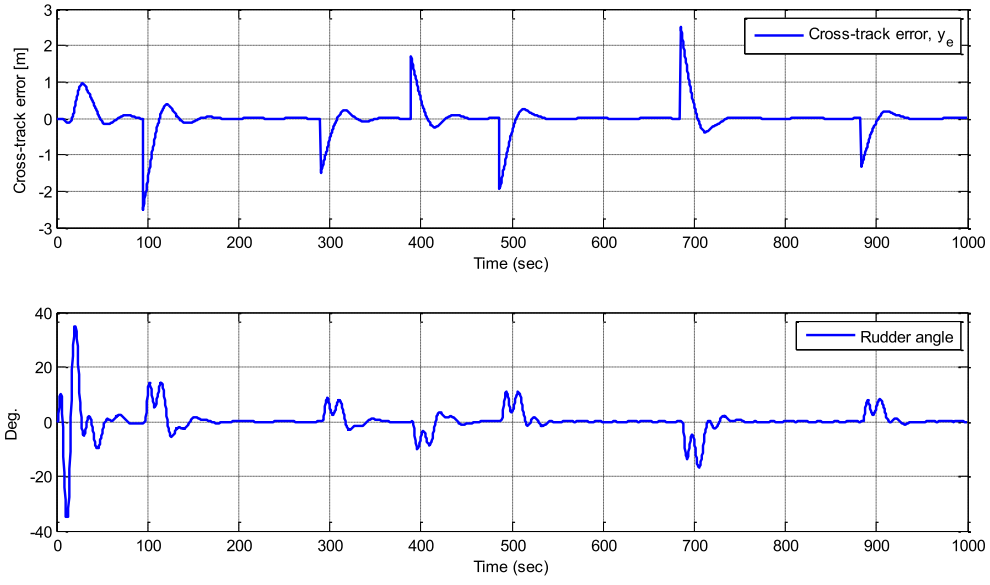

(b) *L1* ON

Fig. 12. The measured cross-track error and rudder angle.

The ship is assumed to start from the origin point. 2D irrotational stochastic ocean current with constant direction ($\beta c = 180^{\circ}$) is considered in the simulation, as shown in Fig. 8. The stochastic ocean current is divided into two phases. A weak ocean current is assumed in the first phase, where the magnitude oscillates around 0.1 m/s. In the second phase, a stronger current is considered, where the mean magnitude is 0.2 m/s.

A saturation is used for rudder dynamics, where the maximum rudder angle is set as 35°. During the simulation, the ship's speed is kept constant, $U_0 = 0.41$ m/s. The ship starts from the initial point, and the initial heading angle is set $\psi_0 = 26^{\circ}$, which equals to the path-tangent angle of predefined path. The initial yaw rate is zero, $r_0 = 0$, and initial rudder angle is zero. The surge speed is controlled using a classical PID controller.

The parameters of the *L1* adaptive backstepping controller are given based on experience. The positive constants, *K1* and K_2, in the control law are given as, $K_1 = 0.02$, $K_2 = 15$. The parameters, Γ_1 and Γ_2, in the state prediction, are given as: $\Gamma_1 = 100^{*} I_Z$, $\Gamma_2 = 10^{*} I_Z$, where I_Z is the inertia moment of the scaled ship model. The initial values of the uncertainties, $\hat{\rho}_\eta, \hat{\sigma}_\eta, \hat{b}^{*}_\eta$, are $\hat{\rho}_\eta = 1, \hat{\sigma}_\eta = 1$ and $\hat{b}^{*}_\eta = 0$. The adaptation gains in Eq. (24) are $\gamma_{\rho_\eta} = 20, \gamma_{\sigma_\eta} = 20, \gamma_{b_\eta} = 10$.

As discussed above, the time-varying function, $\theta(t, y_e)$, plays an important role in guidance law, and affects the overall performance. Here, the time-varying function as chosen as: $\theta(t, y_e) = 0.05|y_e| + 1$. As can be observed, it increases with the variable y_e, and it is continuous, positive. The minimum of the function is 1. So this time-varying function fulfils the Definition 1. The vector field

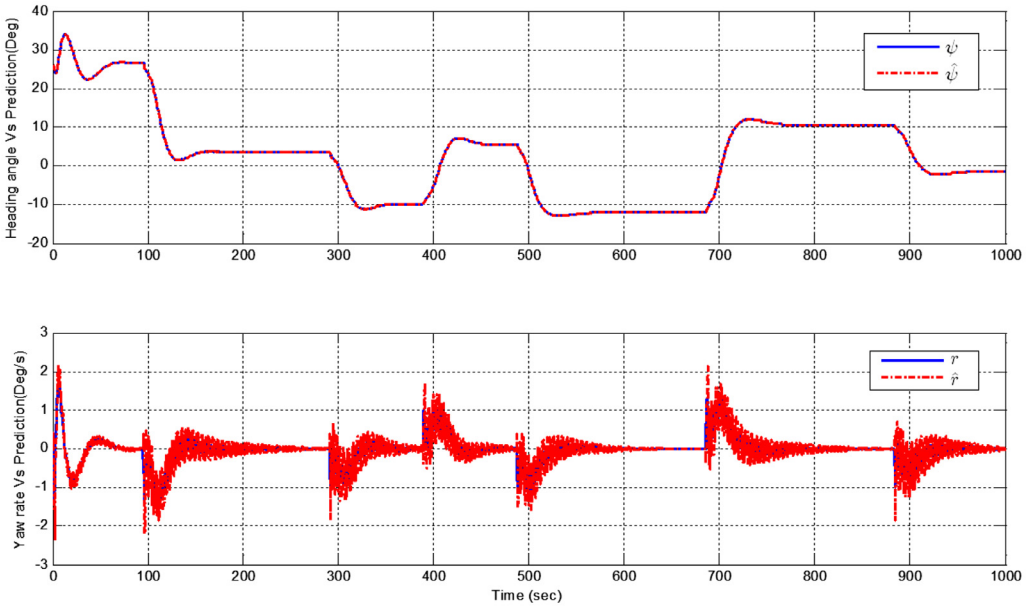

(a) *L1* OFF

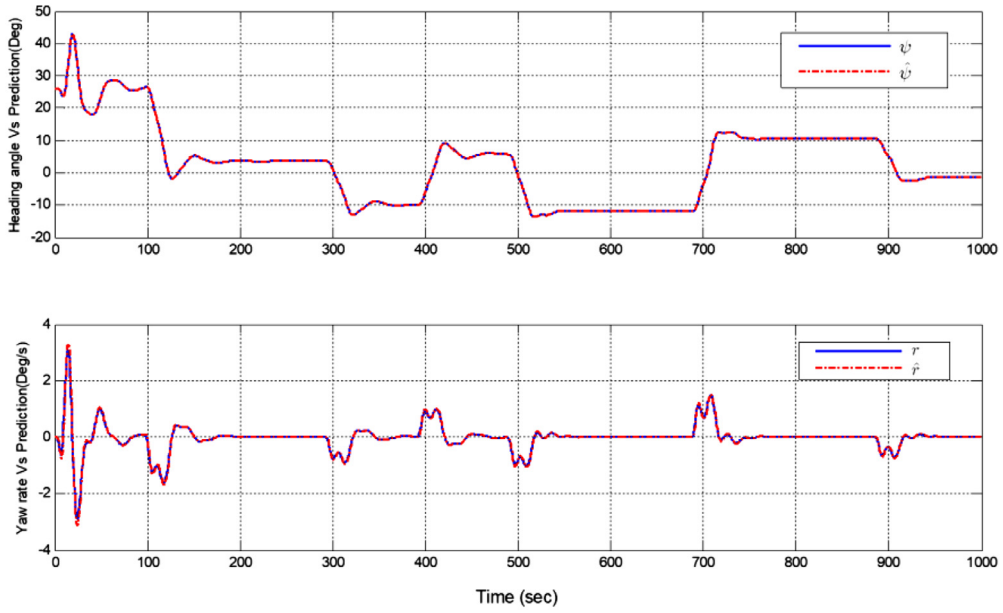

(b) *L1* ON

Fig. 13. The predictions of the heading angle and yaw rate versus the real values in the simulations.

guidance law is given:

$$\psi_d = \gamma_p - \mathrm{sgn}(y_e)\tan^{-1}\left(\frac{(|y_e|)^{0.05|y_e|+1}}{\Delta}\right) - \beta \tag{48}$$

The predefined parameter is chosen as twice the ship length, $\Delta = 2Lpp$ [10]. The adaptation of the uncertainties usually contains high-frequency signals. These high-frequency signals will easily cause frequently back-and-forth steering of the rudder. High-frequency steering is not desired and impossible to implement in real ships, because, on the one hand, it will make more fuel consumption, and on another hand, the ship rudder is usually steered using a hydraulic system, it cannot respond in time. Here, a second-order low pass filter is employed to eliminate the high-frequency signals. The parameters are $\omega = 0.25$ rad/s and critical damping with $\zeta = 1$. The following simulations will show the effect of the low-pass filter. If the low pass filter is turned off, the proposed controller is a typical adaptive backstepping controller.

Fig. 9 shows the predefined path and the trajectory of the ship model during the simulations. The low pass filler was used in Fig. 9(b), and it is turned off in Fig. 9(a). From the figure, the ship can follow the straight-line path successfully in both cases. It can be concluded that the proposed vector field guidance law and *L1* adaptive backstepping controller works properly.

Fig. 10, shows the performance of the *L1* adaptive backstepping controller during the path-following simulations. Fig. 10(a) shows the results when the low pass filter was turned off. The desired and true values of the heading angle are presented in Fig. 10. The autopilot can track the desired heading angles. The surge velocities

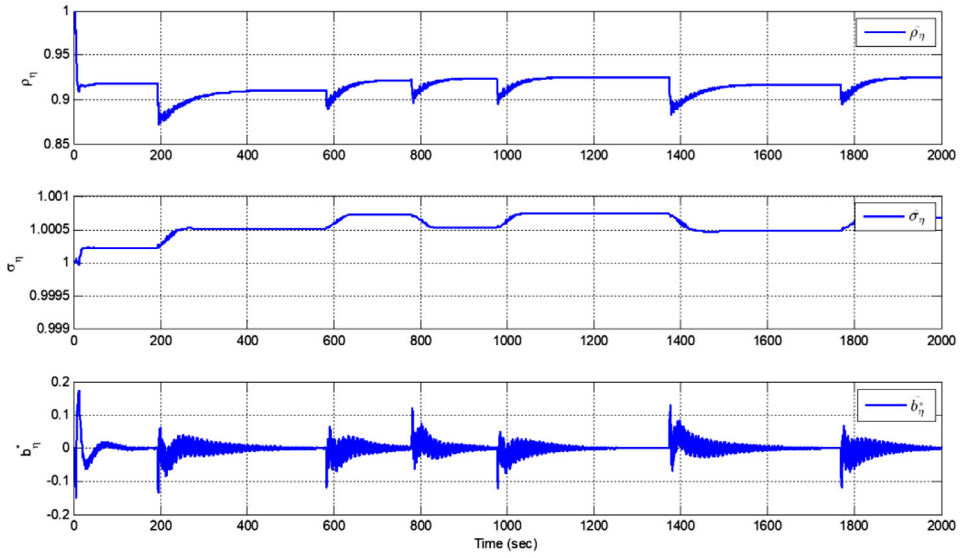

(a) *L1* OFF

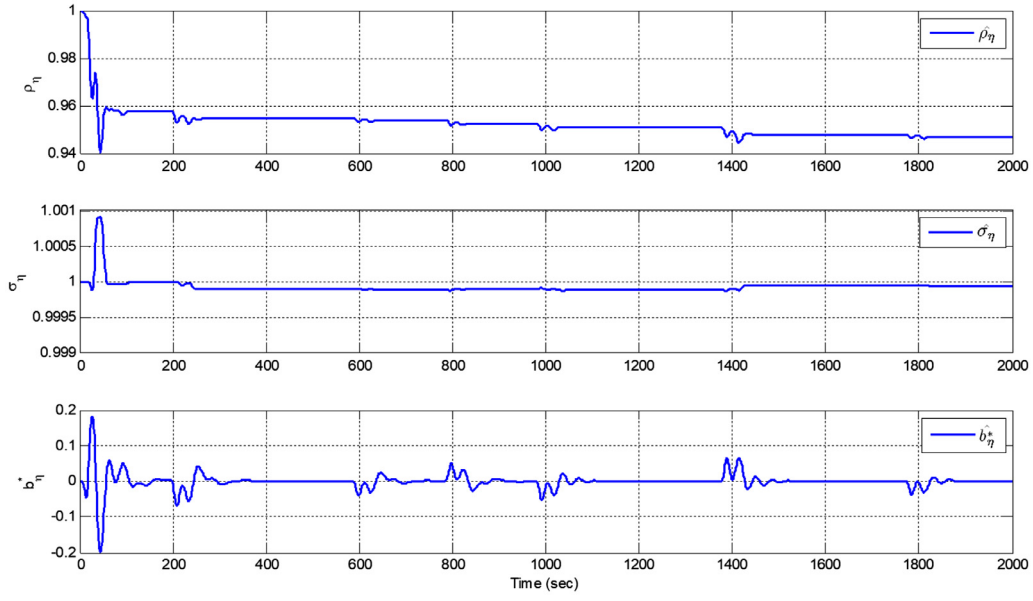

(b) *L1* ON

Fig. 14. The evaluations of the parameters in the simulations.

in simulations are also presented in Fig. 10. The ship can keep a constant surge speed during the simulations. The sway speed in both cases is also given in Fig. 10. As can be observed from the figure, the fluctuation of sway speed is larger when the low pass filter is turned off, as presented in Fig. 10(a). This results from the high-frequency rudder steering when the low pass filter was turned off. It can also be observed in Fig. 11, which shows the course angle (desired versus true) and drift angle for both cases. In Fig. 11(a), the drift angle has a large oscillation without the low-pass filter. The sway speed is related to the drift angle. Usually, the large fluctuation of sway speed or drift angle indicated that the ship was steering a lot to stabilize the system. This high-frequency steering output is due to the adaptation of the uncertainties.

Fig. 12 shows the cross-track errors and rudder angles in the simulations. Obviously, when the low pass filter is turned off, the rudder angle contains the high-frequency signals, which induced by the adaption of the uncertainty. In both cases, the cross-track errors are nearly same. This is because the cross-track error dynamics in Eq. (40) are directly affected by the guidance law and heading error. In both cases, the ship can track the predefined path, but, the rudder angle is more stable when the low pass filter is turned on.

Fig. 13 shows the state predictor of the yaw angle and yaw rate in the simulations. The estimations of the yaw angle ($\hat{\psi}$) and yaw rate ($\hat{r}$) agrees well with the real values. The evaluations of the parameters, $\hat{\rho}_\eta, \hat{\sigma}_\eta, \hat{b}^*_\eta$, are presented in Fig. 14. When the low pass filter was turned off, as presented in Fig. 13(a), the parameters $\hat{\rho}_\eta, \hat{\sigma}_\eta, \hat{b}^*_\eta$ contains high-frequency signals, especially the $\hat{b}^*_\eta$, which represented the environmental disturbance and unmodeled dynamics.

In order to show its effective performance of the $L1$ adaptive backstepping controller, the classical PID controller was used

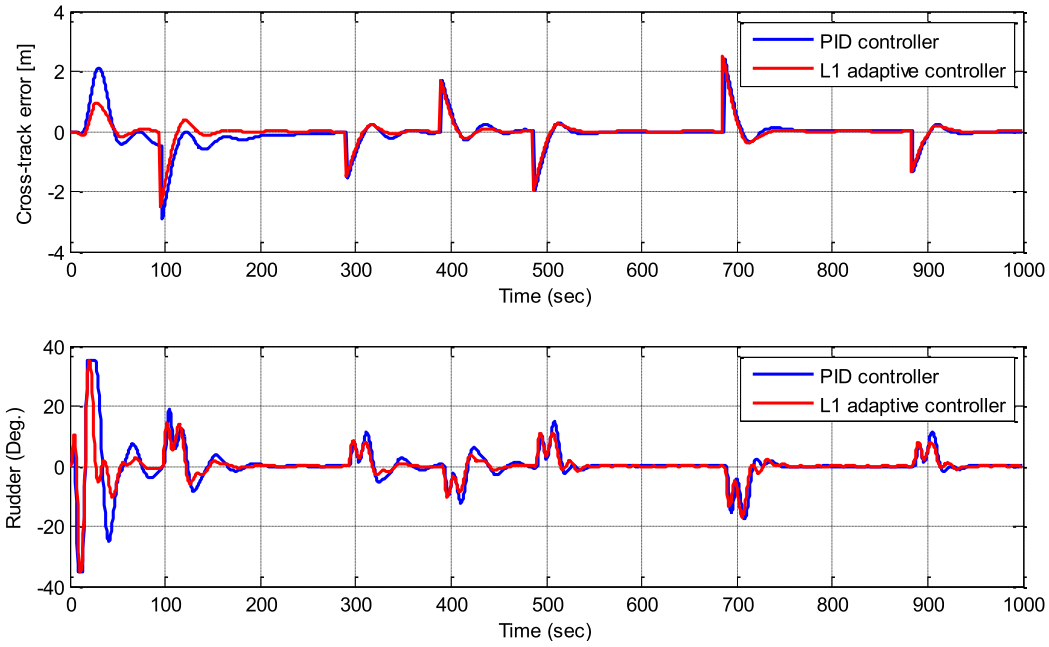

Fig. 15. The cross-track error (above) and rudder angles (below) compared with the classical PID controller for path-following.

in the previous simulations. The predefined parameters and waypoints are same with the previous simulations. The parameters for the PID controller are chosen as: $K_p = \omega_n^2 T/K$; $K_d = (2\zeta\omega_n T - 1)/K$; $K_i = \omega_n^3 T/(10K)$ [10], where ω_n is the natural frequency and ζ is the relative damping ratio of the first order system. In this case, $\omega_n = 1$ rad/s and critical damping with $\zeta = 1$. The cross-track error and rudder angles are plotted in Fig. 15. As can be observed, the PID controller takes more time to converge. The L1 adaptive backstepping controller response fast and have a better performance.

6. Conclusions

In this paper, *L1* adaptive backstepping controller was proposed for path-following control of autonomous ships. *L1* adaptive backstepping was designed based on nonlinear steering model. The parameter update laws and control law were derived using Lyapunov functions. The stability proof shows that the equilibrium point of the error system, $(\tilde{\psi}, \tilde{r}, z_1, z_2, \tilde{\rho}_\eta, \tilde{\sigma}_\eta, \tilde{b}_\eta^*)$, is uniformly globally asymptotically stable. A novel time-varying vector field guidance law was proposed in this paper. It formed a cascade system with the control system. The whole guidance and control system were proved to be uniformly global asymptotically stable using cascade system theory. A theorem and proof were given to guarantee stability performance.

The effectiveness of the proposed control law and vector field guidance law was assessed with a fully nonlinear manoeuvring model of an underactuated tanker in the presence of stochastic ocean current. This manoeuvring model has been validated with experiments and it gave confidence to the results. The results obtained indicated that the proposed heading controller and guidance law can control the underactuated ship to follow the path, while rejecting the environmental disturbance. The low pass filter can eliminate the unnecessary high-frequency signals, which were caused by the adaptation of the uncertainties, in the control input. This paper investigates the important system, guidance and control, of autonomous ships. The proposed time-varying guidance law and the adaptive controller can improve the performance of the autonomous ship in a complex environment, such as shallow water, confined waterway etc. The proposed system can also be used for other autonomous vehicles.

Declaration of Competing Interest

There are no conflicts of interest.

Acknowledgement

This work contributes to M&MSHIPS -“manoeuvring & Moored SHIPS in ports” (PTDC/EMSTRA/5628/2014), funded by the Portuguese Foundation for Science and Technology. This work also contributes to the Strategic Research Plan of the Centre for Marine Technology and Ocean Engineering (CENTEC), which is financed by the Portuguese Foundation for Science and Technology (Fundação para a Ciência e Tecnologia - FCT) under contract UIDB/UIDP/00134/2020.

Appendix A. Proof of Theorem 1

Proof. . As presented in Eq. (14), it can be observed, the subfunction, $|\frac{\sin(x)}{x}| \leq 1$, and $|\frac{\cos(x)-1}{x}| \leq 0.73$, are upper bounded, and,

$$\left|\frac{|y_e|^{\theta(t,y_e)}}{\sqrt{\Delta^2+|y_e|^{2\theta(t,y_e)}}}\right| \leq 1; \text{and} \left|\frac{\Delta}{\sqrt{\Delta^2+|y_e|^{2\theta(t,y_e)}}}\right| \leq 1, \text{where}, 0 < \Delta_{\min} < \Delta < \Delta_{\max} \tag{A1}$$

Then, the function, $\phi(t, y_e, \tilde{\psi})$, is upper bounded, $\phi(t, y_e, \tilde{\psi}) \leq c$ for all y_e and $\tilde{\psi}$.

$$\left|\frac{|y_e|^{\theta(t,y_e)}}{\sqrt{\Delta^2+|y_e|^{2\theta(t,y_e)}}}\right| \leq 1; \text{and} \left|\frac{\Delta}{\sqrt{\Delta^2+|y_e|^{2\theta(t,y_e)}}}\right| \leq 1 \tag{A2}$$

Then, the function,$\phi(t, y_e, \tilde{\psi})$, is upper bounded [12].

As discussed in Section 3, the equilibrium point of the heading autopilot system Σ_2 given by Eq. (40) is UGAS. The nominal system

of the driven system Σ_1 (Σ_1 system with $\tilde{\psi}=0$) is:

$$\dot{y}_e = -\mathrm{sgn}(y_e)\frac{U|y_e|^{\theta(t,y_e)}}{\sqrt{\Delta^2+|y_e|^{2\theta(t,y_e)}}} \tag{A3}$$

The function $\theta(t,y_e)$ is time-varying, so the nominal system in Eq. (A3) is nonautonomous. Consider the CLF,

$$V_1(t,y_e)=\frac{1}{2}y_e^2 \tag{A4}$$

where $V_1(t,y_e)>0$ if $y_e\neq 0$. The time derivative of $V_1(t,y_e)$ is given:

$$\dot{V}_1(t,y_e) = -\mathrm{sgn}(y_e)y_e\frac{U|y_e|^{\theta(t,y_e)}}{\sqrt{\Delta^2+|y_e|^{2\theta(t,y_e)}}} = -\frac{U|y_e|^{\theta(t,y_e)+1}}{\sqrt{\Delta^2+|y_e|^{2\theta(t,y_e)}}} \leq 0 \tag{A5}$$

since $V_1(t,y_e)>0$ and $\dot{V}_1(t,y_e)\leq 0$, according to the Theorem 4.9 by Khalil [25], the equilibrium point, $y_e=0$, is globally uniformly asymptotically stable (UGAS). Moreover, every trajectory starting in $\{x\in B_r\}$ and $B_r=\{\|x\|\leq r\}$, satisfies

$$|y_e(t)|\leq \beta(\|y_e(t_0)\|,t-t_0)\forall t\geq t_0\geq 0 \tag{A6}$$

Then, the cross tracked error is globally bounded and it will globally asymptotically converge to zero. Finally, the equilibrium point ($y_e=0$, $\tilde{\psi}=0$) of the cascaded system described by (39)-(40) is UGAS [6,12,13,34].

References

[1] Allianz Global Corporate and SpecialitySafety and Shipping 1912–2012, Cardiff University, 2012.

[2] P. Batista, C. Silvestre, P. Oliveira, Globally exponentially stable attitude observer with Earth velocity estimation, Asian J. Control (2019) asjc.2056, doi:10.1002/asjc.2056.

[3] W. Caharija, K.Y. Pettersen, P. Calado, J. Braga, A comparison between the ILOS guidance and the vector field guidance, in: Proceedings of the IFAC-PapersOnLine, Elsevier, 2015, pp. 89–94, doi:10.1016/j.ifacol.2015.10.263.

[4] A. Chaillet, A. Loría, Uniform global practical asymptotic stability for time-varying cascaded systems, Eur. J. Control 12 (2006) 595–605, doi:10.3166/ejc.12.595-605.

[5] K. Do, J. Pan, Control of Ships and Underwater Vehicles, Springer, Australia, 2009, doi:10.1007/978-1-84882-730-1.

[6] K.D. Do, Global robust adaptive path-tracking control of underactuated ships under stochastic disturbances, Ocean Eng. 111 (2016) 267–278, doi:10.1016/j.oceaneng.2015.10.038.

[7] K.D. Do, Z.P. Jiang, J. Pan, Robust adaptive path following of underactuated ships, Automatica (2004), doi:10.1016/j.automatica.2004.01.021.

[8] K.D. Do, J. Pan, Global robust adaptive path following of underactuated ships, Automatica (2006a), doi:10.1016/j.automatica.2006.04.026.

[9] K.D. Do, J. Pan, Underactuated ships follow smooth paths with integral actions and without velocity measurements for feedback: theory and experiments, IEEE Trans. Control Syst. Technol. (2006b), doi:10.1109/TCST.2005.863665.

[10] T.I. Fossen, Handbook of Marine Craft Hydrodynamics and Motion Control, John Wiley & Sons, Ltd, Chichester, UK, 2011, doi:10.1002/9781119994138.

[11] T.I. Fossen, A survey on Nonlinear Ship Control: from Theory to Practice, IFAC Proc. 33 (2000) 1–16, doi:10.1016/S1474-6670(17)37044-1.

[12] T.I. Fossen, A.M. Lekkas, Direct and indirect adaptive integral line-of-sight path-following controllers for marine craft exposed to ocean currents, Int. J. Adapt. Control Signal Process. 31 (2015) 445–463, doi:10.1002/acs.2550.

[13] T.I. Fossen, K.Y. Pettersen, On uniform semiglobal exponential stability (USGES) of proportional line-of-sight guidance laws, Automatica 50 (2014) 2912–2917, doi:10.1016/J.AUTOMATICA.2014.10.018.

[14] T.I. Fossen, K.Y. Pettersen, R. Galeazzi, Line-of-sight path following for dubins paths with adaptive sideslip compensation of drift forces, IEEE Trans. Control Syst. Technol. 23 (2015) 820–827, doi:10.1109/TCST.2014.2338354.

[15] E. Fredriksen, K.Y. Pettersen, Global κ-exponential way-point maneuvering of ships: theory and experiments, Automatica 42 (2006) 677–687, doi:10.1016/J.AUTOMATICA.2005.12.020.

[16] I.M. Gregory, C. Cao, E. Xargay, N. Hovakimyan, X. Zou, L1 adaptive control design for NASA AirSTAR flight test vehicle, in: Proceedings of the AIAA Guidance, Navigation, and Control Conference and Exhibit, 2009, doi:10.2514/6.2009-5738.

[17] C. Guedes Soares, A.P. Teixeira, Risk assessment in maritime transportation, Reliab. Eng. Syst. Saf. 74 (3) (2001) 299–309.

[18] C. Guedes Soares, A.P. Teixeira, P. Antao, Accounting for human factors in the analysis of maritime accidents, in: M. Cottam, D. Harvey, R. Pape, J. Tait (Eds.), Foresight and Precaution, Rotterdam, Balkema, 2000, pp. 521–528.

[19] B.J. Guerreiro, C. Silvestre, R. Cunha, C. Cao, N. Hovakimyan, L1adaptive control for autonomous rotorcraft, in: Proceedings of the American Control Conference, 2009, doi:10.1109/ACC.2009.5159940.

[20] J. Guerrero, J. Torres, V. Creuze, A. Chemori, Trajectory tracking for autonomous underwater vehicle: an adaptive approach, Ocean Eng 172 (2019) 511–522, doi:10.1016/J.OCEANENG.2018.12.027.

[21] N. Hovakimyan, C. Cao, L1 adaptive control theory : guaranteed robustness with fast adaptation, Soc. Ind. Appl. Math. (2010).

[22] W. Hwang, Application of System Identification to Ship Maneuvering, Institute of Technology, Massachusetts, 1980.

[23] I. Kaminer, A. Pascoal, E. Xargay, N. Hovakimyan, C. Cao, V. Dobrokhodov, Path following for small unmanned aerial vehicles using L1 adaptive augmentation of commercial autopilots, J. Guid. Control. Dyn. (2010a), doi:10.2514/1.42056.

[24] I. Kaminer, A. Pascoal, E. Xargay, N. Hovakimyan, C. Cao, V. Dobrokhodov, Path following for unmanned aerial vehicles using L1 adaptive augmentation of commercial autopilots, J. Guid. Control. Dyn. (2010b), doi:10.2514/1.42056.

[25] H.K. Khalil, Nonlinear Systems, Prentice Hall, 2002.

[26] E. Lataire, M. Vantorre, G. Delefortrie, M. Candries, Mathematical modelling of forces acting on ships during lightering operations, Ocean Eng. 55 (2012) 101–115, doi:10.1016/J.OCEANENG.2012.07.029.

[27] D.A. Lawrence, E.W. Frew, W.J. Pisano, Lyapunov vector fields for autonomous unmanned aircraft flight control, J. Guid. Control. Dyn. 31 (2008) 1220–1229, doi:10.2514/1.34896.

[28] C. Lee, M. Tahk, B. Jun, Autopilot design for an agile missile using L1 adaptive backstepping control, in: Proceedings of the 28th Congress of the International Council of the Aeronautical Sciences, Brisbane, Australia, 2012.

[29] A.M. Lekkas, T.I. Fossen, Integral LOS path following for curved paths based on a monotone cubic hermite spline parametrization, IEEE Trans. Control Syst. Technol. 22 (2014) 2287–2301, doi:10.1109/TCST.2014.2306774.

[30] A.M. Lekkas, T.I. Fossen, A time-varying lookahead distance guidance law for path following, in: IFAC Proceedings Volumes (IFAC-PapersOnline), 2012, pp. 398–403, doi:10.3182/20120919-3-IT-2046.00068.

[31] M. Li, T. Li, X. Gao, Q. Shan, C.L.P. Chen, Y. Xiao, Adaptive NN event-triggered control for path following of underactuated vessels with finite-time convergence, Neurocomputing 379 (2020) 203–213, doi:10.1016/j.neucom.2019.10.044.

[32] S. Lim, W. Jung, H. Bang, Vector field guidance for path following and arrival angle control, in: Proceedings of the International Conference on Unmanned Aircraft Systems, ICUAS, IEEE, 2014, pp. 329–338, doi:10.1109/ICUAS.2014.6842271.

[33] C. Liu, J. Sun, Z. Zou, Integrated line of sight and model predictive control for path following and roll motion control using rudder, J. Sh. Res. 59 (2015) 99–112, doi:10.5957/JOSR.59.2.140057.

[34] A. Loría, E. Panteley, Cascaded nonlinear time-varying systems: analysis and design, in: F. Lamnabhi-Lagarrigue, A. Loría, E. Panteley (Eds.), Advanced Topics in Control Systems Theory: Lecture Notes from FAP 2004, Springer London, London, 2005, pp. 23–64, doi:10.1007/11334774_2.

[35] K. Maritime (2016). World's first official test bed for autonomous shipping opens in Norway [WWW Document]. URL https://www.km.kongsberg.com/ks/web/nokbg0238.nsf/AllWeb/166309633F206651C125804200250951?OpenDocument (accessed 9.6.18).

[36] S. Moe, K.Y. Pettersen, Set-based Line-of-Sight (LOS) path following with collision avoidance for underactuated unmanned surface vessel, in: Proceedings of the 24th Mediterranean Conference on Control and Automation, MED 2016, 2016, pp. 402–409, doi:10.1109/MED.2016.7535964.

[37] L. Moreira, T.I. Fossen, C. Guedes Soares, Path following control system for a tanker ship model, Ocean Eng. 34 (2007) 2074–2085, doi:10.1016/j.oceaneng.2007.02.005.

[38] D.R. Nelson, D.B. Barber, T.W. McLain, R.W. Beard, Vector field path following for small unmanned air vehicles, in: Proceedings of the American Control Conference, 2006, pp. 5788–5794, doi:10.1109/ACC.2006.1657648.

[39] S.-R. Oh, J. Sun, Path following of underactuated marine surface vessels using line-of-sight based model predictive control, Ocean Eng. 37 (2010) 289–295, doi:10.1016/j.oceaneng.2009.10.004.

[40] E. Panteley, A. Loria, On global uniform asymptotic stability of nonlinear time-varying systems in cascade, Syst. Control Lett. 33 (1998) 131–138, doi:10.1016/S0167-6911(97)00119-9.

[41] E. Panteley, A. Loría, A. Sokolov, Global uniform asymptotic stability of cascaded non-autonomous non-linear systems: application to stabilisation of a diesel engine, Eur. J. Control 5 (1999) 107–115, doi:10.1016/S0947-3580(99)70145-7.

[42] L.P. Perera, C. Guedes Soares, Pre-filtered sliding mode control for nonlinear ship steering associated with disturbances, Ocean Eng. 51 (2012) 49–62.

[43] L.P. Perera, P. Oliveira, C. Guedes Soares, System identification of nonlinear vessel steering, J. Offshore Mech. Arct. Eng. 137 (2015) 031302, doi:10.1115/1.4029826.

[44] L.P. Perera, P. Oliveira, C. Guedes Soares, System identification of vessel steering with unstructured uncertainties by persistent excitation maneuvers, IEEE J. Ocean. Eng. 41 (3) (2016) 515–528.

[45] [45]Rolls-Royce, (2015). Rolls-Royce to Lead Autonomous Ship Research Project [WWW Document]. URL https://www.rolls-royce.com/media/our-stories/press-releases/2015/pr-02-07-15-rolls-royce-to-lead-autonomous-ship-research-project.aspx (accessed 9.6.18).

[46] T.A. Santos, C. Guedes Soares, Economic feasibility of an autonomous container ship, in: C. Guedes Soares, A.P. Teixeira (Eds.), Maritime Transporta-

tion and Harvesting of Sea Resources, Taylor & Francis, London, 2018, pp. 861–870.
[47] M.E.N. Sørensen, M. Breivik, Comparing nonlinear adaptive motion controllers for marine surface vessels, in: Proceedings of the IFAC-PapersOnLine, Elsevier, 2015, pp. 291–298, doi:10.1016/j.ifacol.2015.10.295.
[48] M. Vantorre, Manoeuvring coefficients for a container carrier in shallow water: an evaluation of semi-empirical formulae, in: Proceedings of the Mini Symposium on Prediction of Ship Manoeuvring Performance, Tokyo, Japan, 2001 18 October 2001.
[49] N. Wang, Z. Sun, J. Yin, Z. Zheng, Surge-varying LOS based path following control of underactuated marine vehicles with accurate disturbance observation, in: Proceedings of the IEEE 7th International Conference on Underwater System Technology: Theory and Applications (USYS), IEEE, 2017, pp. 1–6, doi:10.1109/USYS.2017.8309464.
[50] N. Wang, Z. Sun, J. Yin, Z. Zou, S.F. Su, Fuzzy unknown observer-based robust adaptive path following control of underactuated surface vehicles subject to multiple unknowns, Ocean Eng. (2019) 57–64, doi:10.1016/j.oceaneng.2019.02.017.
[51] X. Xiang, C. Yu, L. Lapierre, J. Zhang, Q. Zhang, Survey on fuzzy-logic-based guidance and control of marine surface vehicles and underwater vehicles, Int. J. Fuzzy Syst. 20 (2018) 572–586, doi:10.1007/s40815-017-0401-3.
[52] H. Xu, T.I. Fossen, C. Guedes Soares, Uniformly semiglobally exponential stability of vector field guidance law and autopilot for path-following, Eur. J. Control 53 (2019a) 88–97, doi:10.1016/j.ejcon.2019.09.007.
[53] H. Xu, C. Guedes Soares, Vector field path following for surface marine vessel and parameter identification based on LS-SVM, Ocean Eng 113 (2016) 151–161, doi:10.1016/j.oceaneng.2015.12.037.
[54] H. Xu, V. Hassani, C. Guedes Soares, Uncertainty analysis of the hydrodynamic coefficients estimation of a nonlinear manoeuvring model based on planar motion mechanism tests, Ocean Eng. 173 (2019b) 450–459, doi:10.1016/j.oceaneng.2018.12.075.
[55] H. Xu, M.A. Hinostroza, C. Guedes Soares, Estimation of hydrodynamic coefficients of a nonlinear manoeuvring mathematical model with free-running ship model tests, Int. J. Marit. Eng. 160 (2018) A-213-A-226, doi:10.3940/rina.ijme.a3.2018.448.
[56] H. Xu, M.A. Hinostroza, V. Hassani, C. Guedes Soares, Real-time parameter estimation of a nonlinear vessel steering model using a support vector machine, J. Offshore Mech. Arct. Eng. 141 (2019c) 061606, doi:10.1115/1.4043806.
[57] H. Xu, H. Rong, C. Guedes Soares, Use of AIS data for guidance and control of path-following autonomous vessels, Ocean Eng. 194 (2019d) 106635, doi:10.1016/j.oceaneng.2019.106635.